

Energy gaps measured by scanning tunneling microscopy

Chen Wang, B. Giambattista, C. G. Slough, and R. V. Coleman
Department of Physics, University of Virginia, Charlottesville, Virginia 22901

M. A. Subramanian

Central Research and Development Department, E. I. DuPont DeNemours and Company, Wilmington, Delaware 19880-0356

(Received 8 December 1989; revised manuscript received 27 June 1990)

A scanning tunneling microscope (STM) has been used to measure energy gaps in the charge-density-wave (CDW) phases of the layer-structure dichalcogenides and in the high-temperature superconductor $\text{Bi}_2\text{Sr}_2\text{CaCu}_2\text{O}_8$. Measured values of Δ_{CDW} at 4.2 K for $2H\text{-TaSe}_2$, $2H\text{-TaS}_2$, and $2H\text{-NbSe}_2$ are 80, 50, and 34 meV giving values of $2\Delta_{\text{CDW}}/k_B T_c$ equal to 15.2, 15.4, and 23.9, indicating strong coupling in these CDW systems. Measured values of Δ_{CDW} at 4.2 K in $1T\text{-TaSe}_2$ and $1T\text{-TaS}_2$ are ~ 150 meV for both materials giving $2\Delta_{\text{CDW}}/k_B T_c \approx 5.8$. STM scans of $\text{Bi}_2\text{Sr}_2\text{CaCu}_2\text{O}_8$ at 4.2 K resolve atoms on the BiO_x layer and show possible variations in electronic structure. The energy gap determined from I versus V and dI/dV versus V curves is in the range 30–35 meV giving values of $2\Delta/k_B T_c \approx 8$. Spectroscopy measurements with the STM can exhibit large zero-bias anomalies which complicate the analysis of the energy-gap structure, but adequate separation has been accomplished.

I. INTRODUCTION

In this paper we report results on the use of scanning tunneling microscopy (STM) to measure energy gaps in charge-density-wave (CDW) materials and superconductors. Using the STM for spectroscopy presents special problems connected with the geometry of an atomic tip in close proximity to an atomically flat surface. When the tunneling distance is on the order of a few angstroms the effective barrier is strongly modified from that expected from considerations of the work functions of the two metals. In general, the effective barrier is substantially reduced at small distances and the I versus V characteristics become increasingly nonlinear due to the low effective barrier. The I versus V curves can also show strong perturbations due to surface or tip irregularities at or near the tip position. These can produce charging effects that lead to rapid variations in the I versus V characteristics of a given junction.

Such variations can be extremely large when using the STM for spectroscopic measurements on the high- T_c superconductors, but can also be observed on tunneling into more perfect surfaces such as those observed on the layer-structure dichalcogenides. The results on the dichalcogenide crystals are reproducible, but require systematic analysis and comparison in order to fully characterize a given STM junction. Factors such as the dependence of barrier height on CDW strength and the presence of zero-bias anomalies (ZBA's) have to be taken into account. Structure due to the CDW energy gap can unambiguously be observed once systematic and reproducible comparisons on a number of layer dichalcogenides have been made.

Zero-bias anomalies of various strengths can be generated by given tip-sample combinations and these have to be separated from the intrinsic gap structure. ZBA's

are not present in selected tip-sample combinations and these junctions can be used as standards in comparing the spectroscopic curves obtained for a series of STM junctions on the same layer chalcogenide compound.

We have previously shown that at liquid-helium temperatures excellent atomic resolution can be obtained for a wide range of layer dichalcogenide materials. The z deflections of the STM due to the atomic and to the CDW structure are both sensitive to the strength of the CDW and to the electronic structure. We have previously demonstrated¹ that systematic and reproducible z deflections can be obtained on cleaved layer dichalcogenide compounds using Pt-Ir tips immersed in liquid helium. The variations in the spectroscopic curves discussed here do correlate with changes in the relative z deflection, but all represent a systematic reproducible series of experiments at the atomic resolution level.

We believe that cleaving the crystal followed by immersion in liquid helium gives a clean reproducible STM junction. The variations observed in the spectroscopic curves are, we believe, associated with the detailed structure of the tip including geometry as well as defects and impurities. The z deflections in all cases are proportional to the strength of the CDW and this in turn gives rise to an intrinsic and systematic change in effective barrier height. In addition the barrier height observed for all layer structures measured shows a systematic increase with the distance from tip to surface. These two barrier characteristics are common to all of the cleaved layer dichalcogenide surfaces studied. Impurities can affect the specific magnitudes, but the correlations with CDW strength and tip surface distance are observed in all cases.

Occasionally we observe giant z deflections where the tip may be making contact with a contaminated surface. We do not use such data in the present analysis.

We present data on a series of CDW materials with a

range of CDW transition temperatures and compare the values of $2\Delta_{\text{CDW}}/k_B T_c$ obtained. The CDW materials all give excellent atomic resolution and show a high degree of surface perfection. The Fermi surfaces of the CDW materials are only partially gapped by the CDW so a substantial density of states remains for applied bias voltages below the gap value. This makes it more difficult to determine precise values of Δ_{CDW} , but reasonably strong structure in the I versus V and conductance versus V curves can be unambiguously identified with the CDW gap. A number of CDW materials with widely different CDW onset temperatures have been measured and a substantial range of $2\Delta_{\text{CDW}}/k_B T_c$ values are observed.

We also present data on STM measurements of the superconducting energy gap in $\text{Bi}_2\text{Sr}_2\text{CaCu}_2\text{O}_8$ single crystals. This material presents a more difficult problem for the STM in obtaining both atomic resolution and spectroscopic information. However, selected runs can show reasonably good atomic resolution as well as a reliable gap structure and we will compare the STM response in these cases with the STM measurements on CDW materials. The Bi-Sr-Ca-Cu-O single crystals were predominantly of the 2212 phase and have T_c 's of ~ 95 K. The measured gap value is estimated to be in the range $\Delta = 30\text{--}35$ meV giving a value of $2\Delta/k_B T_c$ in the range 7.3–8.5.

The atomic and CDW structure in the layer-structure dichalcogenides have been studied extensively^{1–3} by STM and excellent simultaneous resolution of the atomic and CDW modulations has been obtained. The electronic modifications of the local density of states induced by the CDW transitions can be detected⁴ with high sensitivity and the STM shows a systematic response to the strength of the CDW. This paper extends the STM studies to point by point measurements of the characteristic tunnel curves and shows that these are even more sensitive to the precise junction structure than are the images recorded from the two-dimensional surface scans.

In the case of the high-temperature superconductors many types of tunnel junction fabrication techniques, including STM, have been carried out in order to measure a superconducting gap structure. These experiments have been recently reviewed by Kirtley⁵ and show that accurate reproducible characteristic tunnel curves are difficult to obtain. The STM studies of Bi-Sr-Ca-Cu-O single crystals reported in this paper demonstrate that atomic resolution can be obtained at 4.2 K and that in selected cases a relatively clear gap structure can be observed.

II. EXPERIMENTAL TECHNIQUES

The STM used for these studies is a custom-built microscope specifically designed for use at liquid-helium temperatures. The construction has been described in detail in Ref. 1. The tunneling tip is machined from $\text{Pt}_{0.80}\text{Ir}_{0.20}$ wire 0.5 mm in diameter and is mounted in an x - y translator machined from a single piece of piezoelectric material. The crystal is mounted on a piezoelectric bimorph cell clamped to the x - y translator. The STM assembly is 1.25 in. in diameter and is mounted on a stainless-steel tube which allows it to be lowered into a

liquid-helium storage Dewar.

The crystals are mounted on the bimorph and then cleaved in air just before placing the bimorph in the STM assembly. The microscope is then inserted into a chamber at the top of the storage Dewar that is filled with helium gas. The entire microscope assembly is then lowered and immersed in liquid helium.

The layer-structure dichalcogenide crystals have been grown by standard iodine vapor transport techniques using sealed quartz tubes. More details on the conditions used for the growth of the various phases can be found in Ref. 1.

The crystals of $\text{Bi}_2\text{Sr}_2\text{CaCu}_2\text{O}_8$ were supplied by the Central Research and Development Department of E.I. DuPont de Nemours and Company. The crystal used for the data in this paper has a superconducting transition with a T_c estimated to be ~ 95 K and reached zero resistance at 90 K.

The I versus V curves presented in this report were recorded by setting the tip-sample distance by adjusting the STM to a current of 2.2 nA with an applied bias voltage of 75 mV. The error amplifier was then momentarily disconnected while the bias voltage was swept through the designated range. The dI/dV versus V curves were recorded using the same set point, but applying an additional ac frequency of 1 kHz during the dc sweep with an amplitude of 3 mV. The magnitude of dI/dV was detected with a lock-in amplifier. Both characteristic curves were controlled and recorded using an IBM PC-AT computer. The number of sampling points and the number of curves recorded in any data set could be chosen with the computer drive program. The STM scan was displayed at the same time and the position of the tip in the STM scan used for a given characteristic curve was chosen by moving the cursor. An effective tunnel barrier height was calculated by measuring dI/dz at a given current and using the low voltage approximation given in Eqs. (1)–(4). dI/dz can be measured by setting the current and voltage of the STM, and applying an ac voltage to the bimorph in order to produce a calibrated amplitude Δz of ~ 0.1 Å. ΔI is then measured with a lock-in amplifier tuned to the bimorph modulation frequency, usually 1 kHz. The effective barrier height ϕ is calculated using Eq. (4). We write

$$I \propto e^{-A\phi^{1/2}z}, \quad (1)$$

$$\ln I = -A\phi^{1/2}z + \text{const}, \quad (2)$$

$$\phi = A^{-2} \left[\frac{d \ln I}{dz} \right]^2, \quad (3)$$

with ϕ in volts and z in angstroms, $A \simeq 1.025$ and

$$\phi = 0.95 \left[\frac{d \ln I}{dz} \right]^2. \quad (4)$$

The above expressions are approximately valid for $V \ll \phi$ and are derived for parallel-plane electrodes. Therefore applications to the STM data provide only a rough estimate of the barrier-height behavior. By setting the dc current at a constant value and measuring dI/dz at various dc voltages in the range 0–500 mV the barrier

height as a function of tunneling distance z can be measured. At constant dc current z increases as voltage bias increases, but no absolute values of z can be determined at present. The change in distance over the range 5–500 mV is estimated to be $\sim 3 \text{ \AA}$.

III. EXPERIMENTAL RESULTS

Measurements of I versus V and dI/dV (conductance) versus V have been made on a wide range of layer-structure compounds. The CDW's observed in these compounds show a substantial range of onset temperatures and Fermi-surface modifications at the CDW transition. The spectroscopy measurements with the STM are consistent with the major trends expected and show systematic variations in the magnitude of the energy gap as well as in subtle differences related to detailed changes in the Fermi surface. Many of the CDW gaps are comparable in magnitude to those observed in the high- T_c superconductors and STM measurements of the superconducting gaps involve similar problems.

We first discuss results on the $2H$ -phase layer-structure compounds $2H\text{-TaSe}_2$, $2H\text{-TaS}_2$, and $2H\text{-NbSe}_2$. These materials have similar CDW transitions with CDW onset temperatures of 122, 75, and 33 K, respectively. We then discuss data on the $1T$ -phase compounds $1T\text{-TaSe}_2$ and $1T\text{-TaS}_2$ which have CDW onset temperatures at ~ 600 K and much larger CDW gaps. Finally we present STM results on $\text{Bi}_2\text{Sr}_2\text{CaCu}_2\text{O}_8$ single crystals which show a well-defined gap structure, but often exhibit a substantial density of states below the gap. The presence of states below the gap is a sensitive function of the particular crystal cleave and surface condition and is likely to be connected with crystal defects or modifications of the surface layers. Atomic resolution can be obtained with STM scans on Bi-Sr-Ca-Cu-O single crystals at 4.2 K, but substantially more surface irregularity is present than observed for the cleaved layer-structure dichalcogenides. A representative STM scan is presented.

The materials summarized above are all quasi-two-dimensional layered crystals that can be cleaved easily to give large-area atomically flat surfaces.

A. CDW energy gaps in $2H\text{-TaSe}_2$, $2H\text{-TaS}_2$, and $2H\text{-NbSe}_2$

The three $2H$ -phase layer compounds to be compared all form triple q CDW phases with a superlattice wavelength of three times the atomic spacing.⁶ The CDW in $2H\text{-TaSe}_2$ is commensurate below 90 K while in $2H\text{-TaS}_2$ and $2H\text{-NbSe}_2$ the CDW remains slightly incommensurate.

1. $2H\text{-TaSe}_2$

Typical gray-scale STM scans at 4.2 K on $2H\text{-TaSe}_2$ are shown in Fig. 1 for two different crystals and tunneling tips. The individual surface Se atoms are clearly resolved and the CDW superlattice shows up as an enhancement on every third row of atoms. The two scans shown in Fig. 1 have significantly different z deflections with the scan in Fig. 1(b) showing approximately eight times the modulation amplitude as observed in Fig. 1(a).

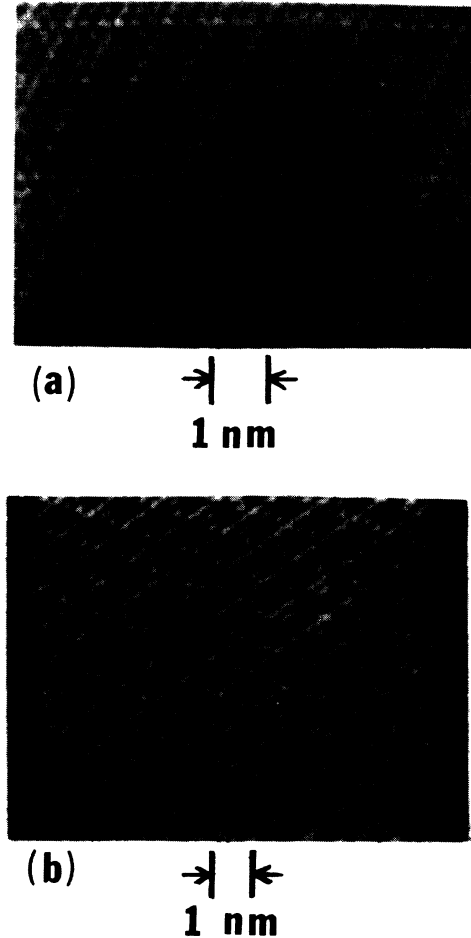


FIG. 1. Gray-scale images of STM scans on two different crystals of $2H\text{-TaSe}_2$ at 4.2 K. The two images show the CDW as an enhancement on every third row of atoms, but differ in total z deflection by a factor of 8 as indicated in the profiles shown in Fig. 2. (a) Scan taken at $I=2.2$ nA and $V=25$ mV. (b) Scan taken at $I=2.2$ nA and $V=75$ mV showing an enhanced CDW modulation and a larger total z deflection.

The corresponding profiles are shown in Fig. 2, and indicate maximum z deflections of 0.10 and 0.80 \AA , respectively. Both scans show a CDW modulation at a wavelength of $3a_0$. However, the scan in Fig. 1(a) and the profile in Fig. 2(a) show that the atomic modulation is dominant while the scan in Fig. 1(b) and the profile in Fig. 2(b) show that the CDW modulation is dominant. This large enhancement of the CDW modulation occurs when the observed z deflection is larger than normal in the $2H$ -phase compounds and is also correlated with the presence of a ZBA and a lower effective barrier height as discussed below.

The more perfect STM scans on $2H\text{-TaSe}_2$ generally show a low z deflection in the range 0.2–0.3 \AA and a correspondingly higher effective barrier height as calculated from measurements of dI/dz versus V using Eq. (4). The effective barrier height versus voltage for the scan shown in Fig. 1(a) is plotted in Fig. 3(a). In most cases the bar-

rier height changes rapidly at low bias voltage where the tip is close to the surface and rises to a saturated value at high voltage where the tip is farther from the surface. The characteristic tunnel curves to be distinguished have been taken at a set point of 75 mV and 2.2 nA which sets the width of the tunnel barrier. In the case of the crystal and tip combination used for the data of Figs. 1(a) and 2(a) the effective barrier height was therefore ~ 1.8 V at the set point as determined from the curve in Fig. 3(a). For the second crystal and tip combination used for the data of Figs. 1(b) and 2(b) the effective barrier height at the set point of 75 mV and 2.2 nA was ~ 0.8 V as determined from the curve in Fig. 3(b). All three 2H-phase materials show gray-scale STM patterns very similar to that shown in Fig. 1 for 2H-TaSe₂, but exhibit systematic differences in total z deflection. The tunnel characteristics as a function of voltage have been measured for surface points corresponding to maxima and minima in both the atomic and CDW modulations. For the materials studied so far we do not detect any variation in tunnel characteristics for different positions of the tip. In addi-

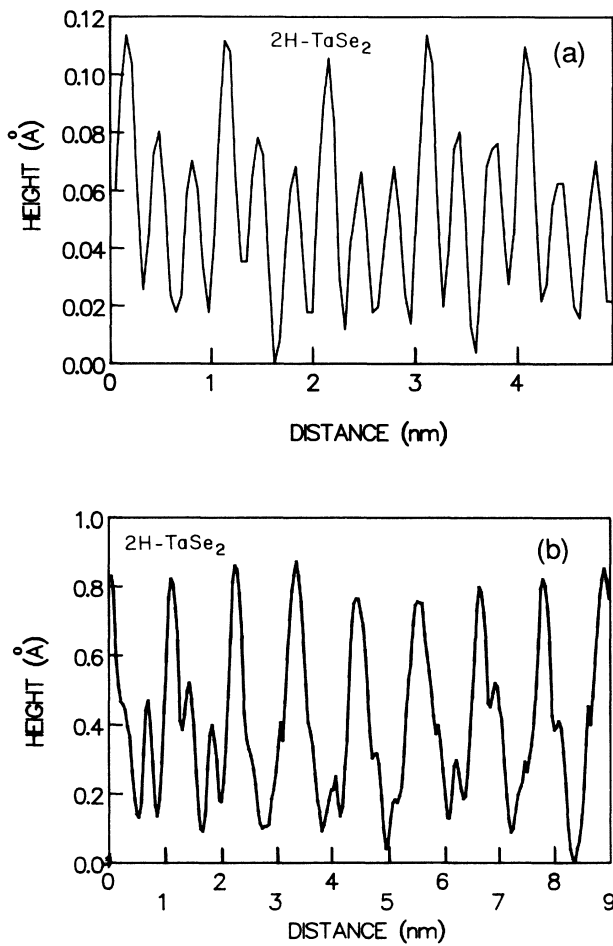


FIG. 2. Profiles of z deflection measured for the two STM scans of 2H-TaSe₂ shown in Fig. 1. (a) Profile with maximum z deflection of ~ 0.1 Å dominated by the atomic modulation. The CDW modulation enhances every third peak. (b) Profile with maximum z deflection of ~ 0.8 Å dominated by the CDW modulation.

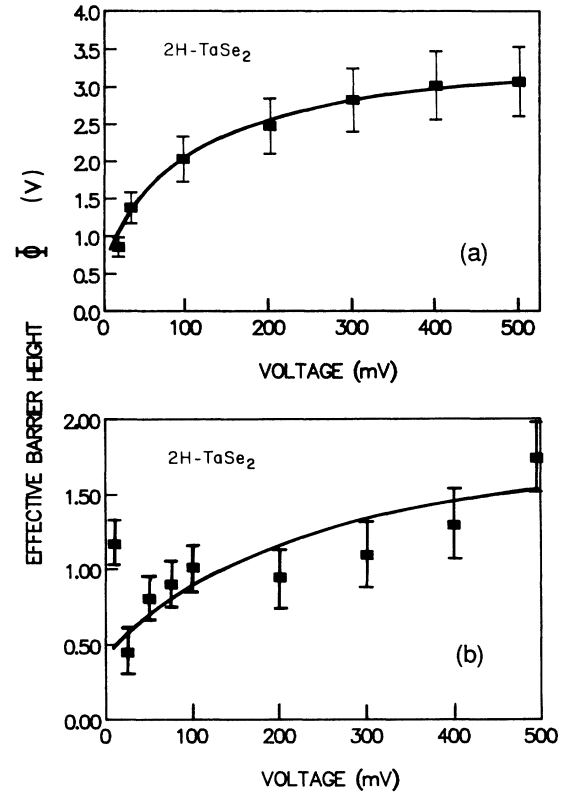


FIG. 3. Effective barrier heights as a function of voltage measured at 4.2 K for the gray-scale images in Fig. 1. The barrier height is determined by measuring dI/dz and using Eq. (4). In this set of experiments increasing voltage corresponds to increasing distance between the tip and surface. (a) For the gray-scale image in Fig. 1(a) the barrier height is observed to saturate around $\phi \sim 3.0$ V and was approximately 2.0 V for the set point at which the scan was taken. (b) For the gray-scale image in Fig. 1(b) the barrier is observed to saturate at $\phi = 1.5$ V and was approximately 0.8 V for the set point at which the scan was taken.

tion, different tunnel distances (set points) change the absolute conductance but do not affect the relative changes in conductance induced by the CDW gap structure.

The dI/dV versus V curves measured for the crystal-tip combinations used for Figs. 1–3 are shown in Fig. 4. The upper conductance curve corresponds to the low z deflection and higher barrier junction [Figs. 1(a), 2(a), and 3(a)]. The relatively abrupt change in slope at ± 80 mV is identified with the CDW gap giving a value of $\Delta_{\text{CDW}} \approx 80$ meV in 2H-TaSe₂. Successive runs on 2H-TaSe₂ at 4.2 K using different crystal-tip combinations consistently show structure and slope changes at ± 80 mV. However, additional structure at lower bias voltages (below 50 mV) is often observed as shown in the lower dI/dV versus V curve of Fig. 4. The overall conductance is substantially suppressed when this structure is present and we associate it with a ZBA giving an additional sharp peak in the dynamic resistance at zero bias.

The I versus V and dynamic resistance (dV/dI) versus

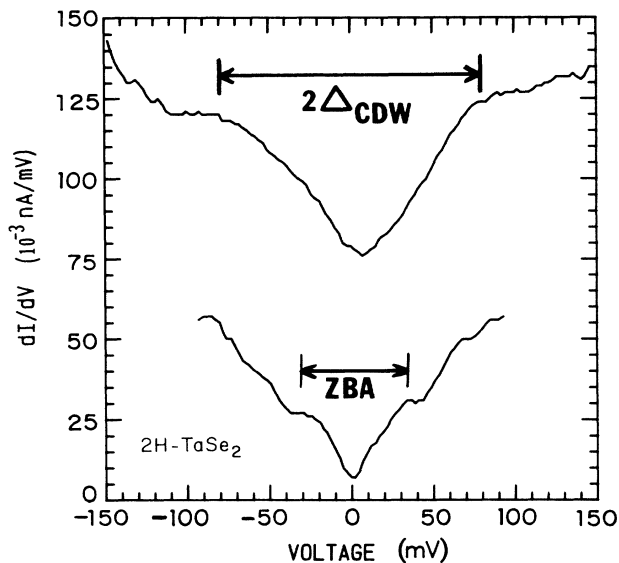


FIG. 4. dI/dV vs V curves for the gray-scale images in Fig. 1. The upper conductance curve was measured on the crystal used in Fig. 1(a) which is the low z deflection, high barrier junction. The relatively sharp break at $\sim \pm 80$ mV is associated with the CDW gap. The lower conductance curve was measured on the crystal used in Fig. 1(b) which is the high z deflection, low barrier junction. Additional structure near zero bias is associated with a ZBA while weak structure associated with the CDW appears at $\sim \pm 80$ mV.

V curves for the two junctions used for the data of Figs. 1–4 are compared in Fig. 5. The large differences in the magnitude and slope of the I versus V curves are reflected in the magnitude and width of the ZBA. The broad maximum of Fig. 5(a) is primarily associated with the CDW gap while the larger and narrower maximum observed in Fig. 5(b) appears to result from a variable ZBA mechanism of unknown origin. The presence of the extra ZBA generally correlates with the observation of a larger z deflection, a lower effective barrier, and a depressed conductance. A reversal in the relative amplitudes of the CDW and atomic modulations can also be observed when a ZBA and low effective barrier height are present. These effects possibly arise from differences in the tip structure and will be discussed further in Sec. IV.

Data as shown above are typical for the CDW materials which remain relatively good metals below the CDW onset temperature. The density of states changes in the vicinity of the gap bias voltage, but the sharpness of the structure and the magnitude of the change observed in the tunnel characteristic depend on the area of Fermi surface (FS) that is gapped. An appreciable density of states remains below the gap edge for materials in which the CDW is relatively weak. In the case of $2H\text{-TaSe}_2$ the band-structure calculations as well as other direct experimental measurements indicate that a substantial FS area and density of states remain in the CDW phase and this information will be reviewed in more detail in Sec. IV.

A better estimate of the tunneling characteristics as modified by the presence of the CDW gap and ZBA's can

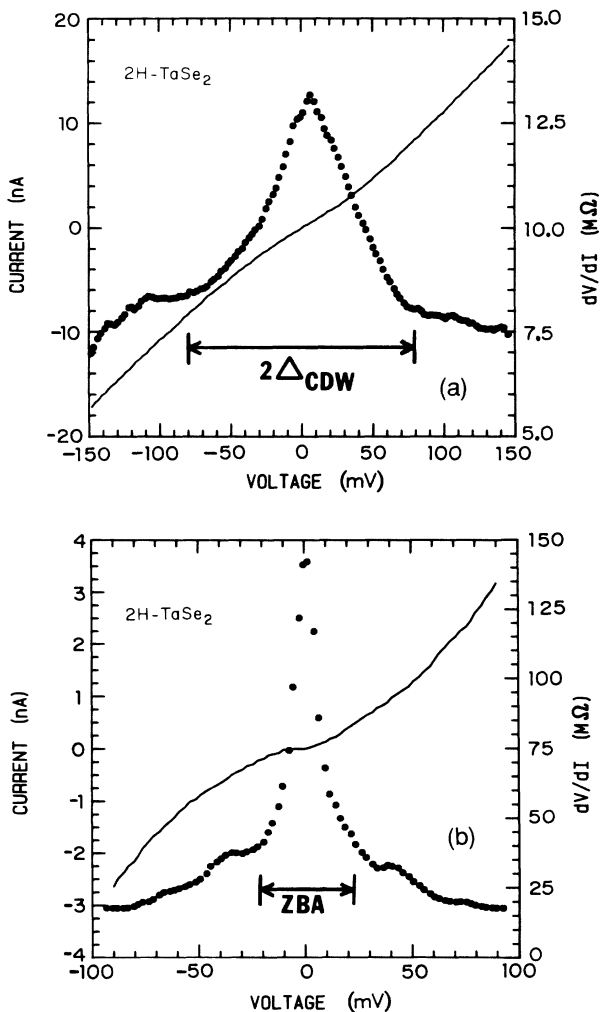


FIG. 5. I vs V and dV/dI (dynamic resistance) vs V curves demonstrating the difference between crystal-tip combinations dominated by the CDW structure and the ZBA structure. (a) Broad maximum and relatively low dynamic resistance dominated by CDW structure. (b) Narrow maximum and high dynamic resistance associated with a dominant ZBA.

be obtained by comparing tunneling data from a number of different CDW materials. Systematic differences as well as similarities can help in the analysis of the tunnel characteristics. The tunneling data on $2H\text{-TaS}_2$ offer a good comparison to the results on $2H\text{-TaSe}_2$ and this comparison is discussed below.

2. $2H\text{-TaS}_2$

The CDW structure and the high-temperature band structure of $2H\text{-TaS}_2$ are very similar to those calculated and observed for $2H\text{-TaSe}_2$. The resistivity shows a very similar weak anomaly at the CDW transition temperature and is of the same order of magnitude in both materials. However, the FS cross sections in the CDW phase of $2H\text{-TaS}_2$ as measured by Shubnikov–de Haas experiments⁷ are an order of magnitude smaller than observed in $2H\text{-TaSe}_2$. This would indicate that a greater

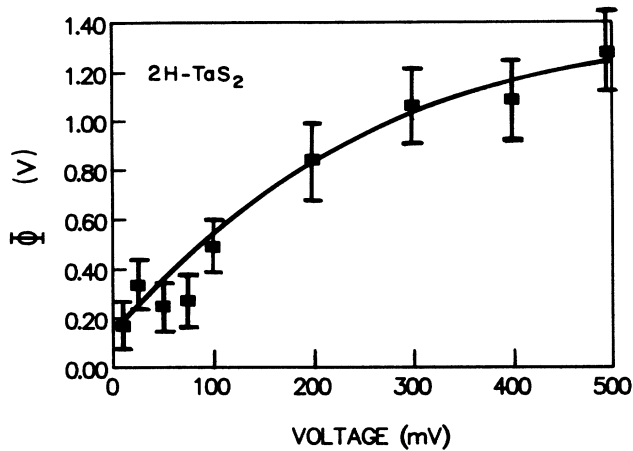


FIG. 6. Effective barrier height vs bias voltage measured on a $2H\text{-TaS}_2$ crystal. At the set point the barrier height is ~ 0.3 V and saturates to a value of ~ 1.4 V.

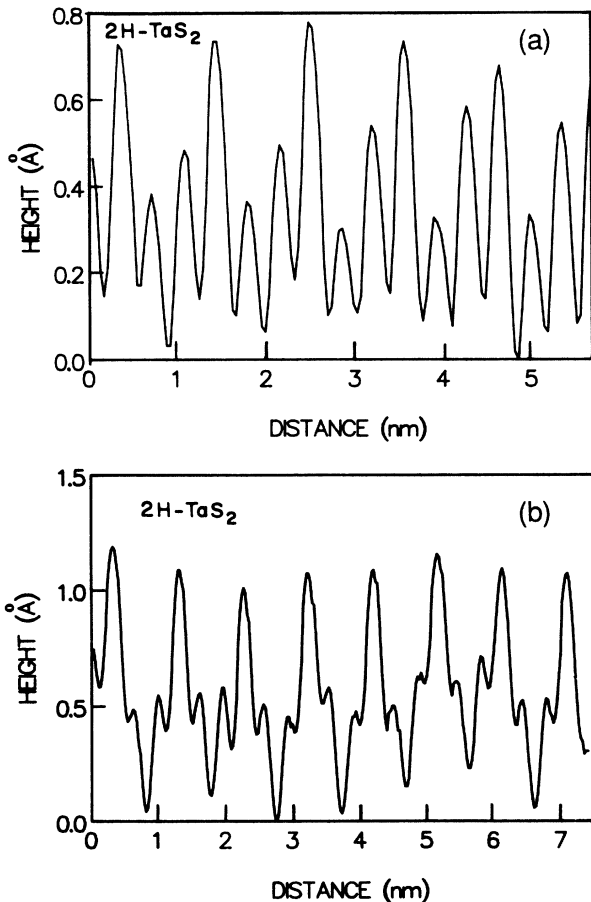


FIG. 7. Profiles of STM scans on $2H\text{-TaS}_2$ at 4.2 K showing the change in relative CDW and atomic modulation amplitudes as the effective barrier height decreases and the total z deflection increases due to the presence of a ZBA. (a) The total z deflection equals ~ 0.7 Å with approximately equal CDW and atomic modulations (no ZBA). (b) The total z deflection equals ~ 1.2 Å and the CDW amplitude is dominant (ZBA).

portion of the high-temperature FS is gapped by the CDW in $2H\text{-TaS}_2$ than in $2H\text{-TaSe}_2$.

The STM scans of $2H\text{-TaS}_2$ consistently show a larger z deflection and a lower effective barrier height than observed for $2H\text{-TaSe}_2$, but can also show an enhanced z deflection and a reduced conductance when a ZBA is present. The barrier height as a function of bias voltage as calculated from Eq. (4) for a typical run is shown in Fig. 6. The effective barrier height at the set point of 75 mV and 2.2 nA is ~ 0.3 V and can vary substantially from run to run. The presence of a reduced barrier height and a ZBA is accompanied by an enhancement of the CDW modulation amplitude relative to the atomic modulation amplitude as demonstrated in Fig. 7. The profile in Fig. 7(a) corresponds to a STM scan with a relatively low z deflection and shows a dominant atomic modulation amplitude. When the z deflection is > 1 Å as shown in the profile of Fig. 7(b) the CDW modulation amplitude is strongly enhanced relative to the atomic modulation.

These large changes in the relative CDW and atomic modulation amplitudes due to low barriers and ZBA's are characteristic of the $2H$ -phase Ta compounds. Such strong relative changes in amplitude are not observed in $2H\text{-NbSe}_2$ with a very weak CDW or in the $1T$ phases of TaSe_2 and TaS_2 with extremely strong CDW's, although substantial ZBA's can also be observed in all of these cases. The characteristic conductance curves in $2H\text{-TaS}_2$ show a systematic behavior similar to that observed for $2H\text{-TaSe}_2$. Two examples are shown in Fig. 8. The upper curve shows an abrupt change in slope below ~ 50 mV which we identify as due to the CDW gap. Other sample-tip combinations can show a much lower conductance at zero bias as shown in the lower curve of Fig. 8.

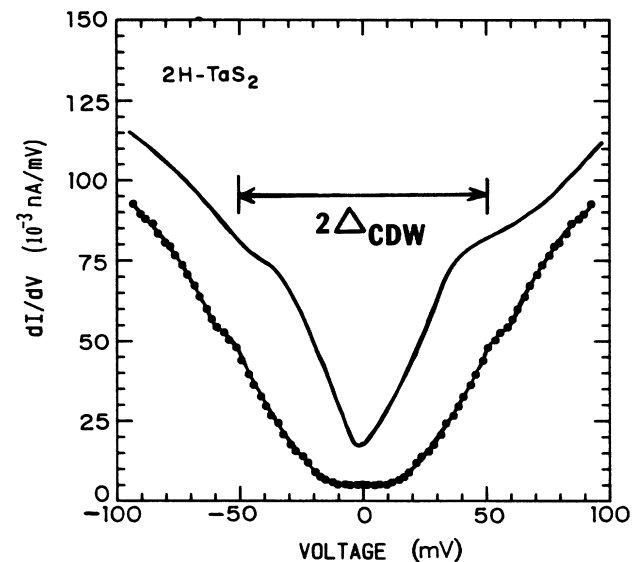


FIG. 8. dI/dV (conductance) vs V curves measured for two different tip-sample combinations. The upper curve shows structure dominated by the CDW with a gap edge at $\sim \pm 50$ mV. The lower curve is dominated by a strong ZBA with only weak structure at $\sim \pm 50$ mV and the conductance is substantially reduced by the ZBA.

Structure is still present at ~ 50 mV but the strong suppression of the conductance tends to reduce the slope change.

The suppression of the conductance can again be assigned to the presence of a ZBA. The I versus V and dV/dI versus V curves corresponding to the lower curve in Fig. 8 are shown in Fig. 9. The ZBA produces a region of nearly zero slope in the I versus V curve near zero bias and a corresponding peak in dynamic resistance. This ZBA region is quite variable, but is generally limited to less than ± 50 mV. All of the curves show the onset of structure and a sharp reduction in conductance below 50 mV. In cases with a weak ZBA the conductance appears to be dominated by the CDW gap and remains relatively high. In cases with a strong ZBA, both the CDW gap and the ZBA contribute and merge and the conductance is strongly suppressed, but weak structure consistent with a CDW gap of ~ 50 mV is still observed.

The measured tunnel characteristics are consistent with a lower density of states below the gap in $2H\text{-TaS}_2$ than in $2H\text{-TaSe}_2$. The conductances at low bias are systematically lower in $2H\text{-TaS}_2$ than in $2H\text{-TaSe}_2$, but quantitative comparisons should be made only on junctions which show no ZBA structure.

3. $2H\text{-NbSe}_2$

$2H\text{-NbSe}_2$ has a CDW onset at ~ 33 K and only a relatively small section⁸ of the total FS area is gapped by the CDW. The STM scans of $2H\text{-NbSe}_2$ at 4.2 K show total z deflections on the order of ~ 0.5 Å in cases exhibiting the most uniform resolution and smallest contribution from a ZBA. A typical gray-scale scan is shown in Fig. 10(a) and a corresponding profile is shown in Fig. 10(b). The atomic and CDW modulations contribute approximately equal amplitudes in this case, but the relative amplitudes can change when larger z deflections and ZBA's

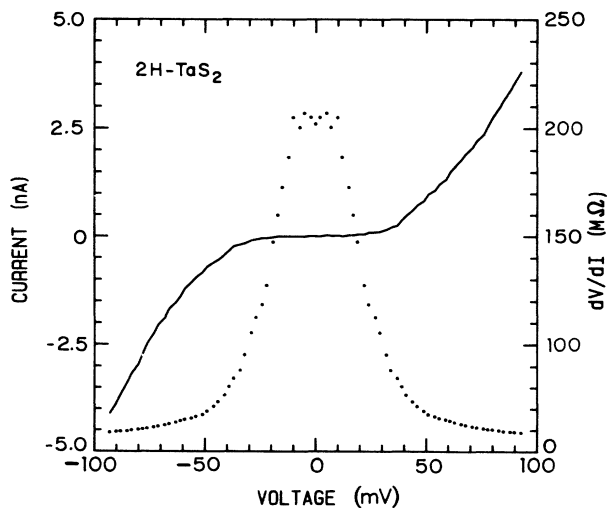


FIG. 9. I vs V and dV/dI vs V corresponding to the lower curve in Fig. 8. The ZBA creates a region of zero slope centered around zero bias and a maximum in dynamic resistance which masks the CDW structure.

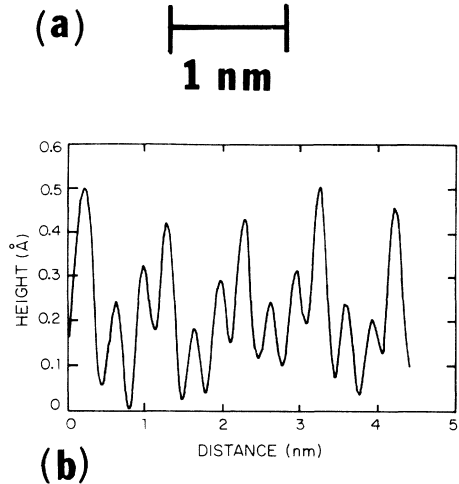
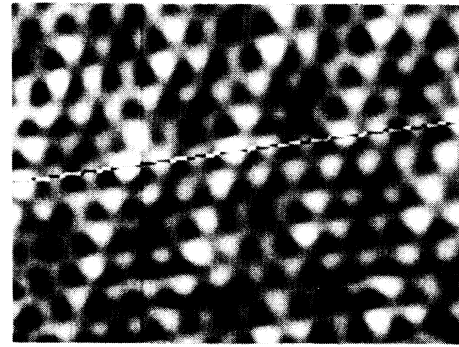


FIG. 10. (a) Gray-scale image of STM scan on $2H\text{-NbSe}_2$ at 4.2 K. ($I=2.0$ nA, $V=25$ mV). The total z deflection is low at ~ 0.5 Å with CDW and atomic modulations of approximately equal magnitudes as shown in the profile in (b) (from Ref. 10).

are present.

The dI/dV versus V curves for two different sample-tip combinations are shown in Fig. 11. The upper conductance curve shows little if any ZBA contribution and the break in slope at ~ 34 mV is associated with the CDW gap in agreement with an independent STM measurement by Hess *et al.*⁹

The lower conductance curve in Fig. 11 exhibits a much stronger ZBA and the entire conductance is suppressed over the bias range shown. Structure near ± 30 mV is again observed, but the presence of the dominant ZBA makes identification of Δ_{CDW} more difficult. An example of a giant ZBA is shown in Fig. 12. In this case the I versus V curve shows a region of zero slope extending to $\sim \pm 50$ mV and any structure due to the CDW gap is completely suppressed. Such a large ZBA is only occasionally observed and reasonably good atomic resolution can still be obtained. The effective barrier heights measured for $2H\text{-NbSe}_2$ show a range of values comparable to those observed for the other $2H$ -phase compounds. The junctions with the lowest z deflections show relatively high effective barrier heights with magnitudes reaching 2–3 V at 500-mV bias. The junctions with large ZBA's and very nonlinear conductance curves generally show large z deflections and low effective barrier heights. The

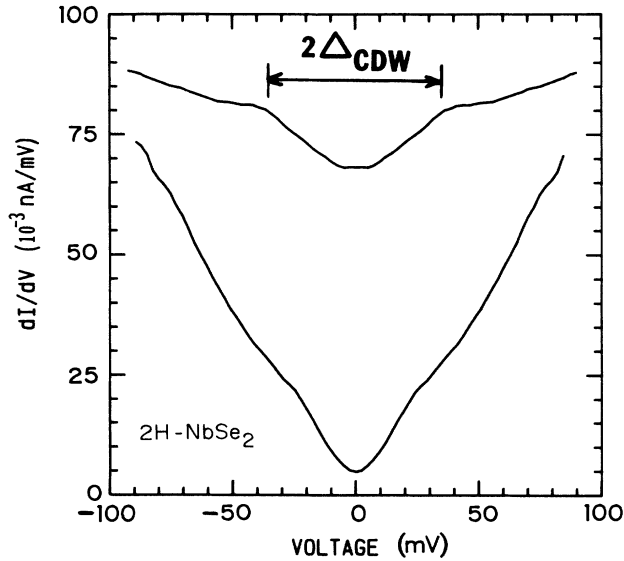


FIG. 11. dI/dV vs V curves measured on $2H\text{-NbSe}_2$ at 4.2 K with two different tip-sample combinations. Upper curve shows dominant CDW structure with a gap edge at $\sim \pm 34$ mV. Lower curve is dominated by a ZBA which substantially depresses the conductance and weakens the CDW gap structure.

barrier height as a function of bias voltage measured for the junction used with the large ZBA (see Fig. 12) is shown in Fig. 13. A very rapid dependence of the barrier height on voltage is observed and the barrier height remains low over the entire bias range up to 500 mV.

The range of behavior demonstrated above for $2H\text{-NbSe}_2$ is similar to that observed for the $2H$ -phase Ta compounds. The presence of ZBA's suppresses the conductance and tends to obscure the direct structure due to the CDW gap. However, selected crystal-tip combina-

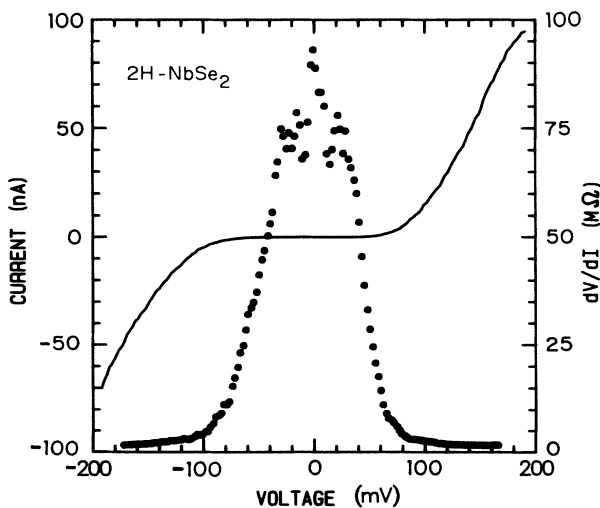


FIG. 12. I vs V and dV/dI vs V curves measured on $2H\text{-NbSe}_2$ with a tip-sample combination exhibiting a giant ZBA extending to $\sim \pm 100$ mV. The CDW structure and gap edge are completely suppressed.

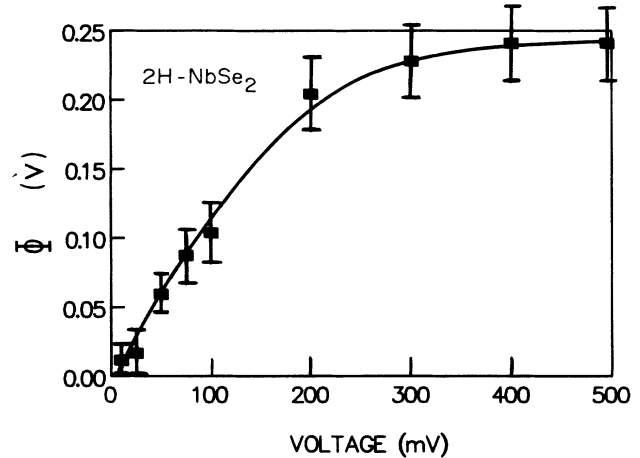


FIG. 13. Effective barrier height vs bias voltage measured on the tip-sample combination exhibiting the giant ZBA shown in Fig. 12. The effective barrier height is a rapid function of bias voltage and remains extremely low over the entire range.

tions show relatively small ZBA's and in these cases the CDW gap structure dominates the conductance and good gap measurements can be made.

B. CDW energy gaps in $1T\text{-TaSe}_2$ and $1T\text{-TaS}_2$

The $1T$ -phase Ta compounds have much larger CDW energy gaps than observed in the $2H$ -phase compounds. ZBA's are also observed and have comparable widths to those observed in the $2H$ compounds. The structure in the characteristic tunnel curves due to the CDW gap edge is therefore at much higher bias voltage and the ZBA causes less interference with the direct observation of the gap edge. The STM scans on the $1T$ -phase junctions with little or no ZBA structure show an average z deflection two to four times greater than observed in the $2H$ -phase compounds. The larger z deflections translate into measurements of lower effective barrier heights and the absolute magnitudes of the barrier heights are also a sensitive function of the barrier width. Different tip-sample combinations can show substantial variations in tunnel conductance at low bias when a ZBA is present. The overall behavior clearly reflects the increased strength of the CDW and the larger energy gap. Further discussion will be given in Sec. IV.

1. $1T\text{-TaSe}_2$

The STM scans of $1T\text{-TaSe}_2$ at 4.2 K are dominated by the CDW superlattice with a spacing of $\sqrt{13}a_0 \times \sqrt{13}a_0$ as shown in the two gray-scale scans of Fig. 14. The two scans shown in Fig. 14 were taken on the same crystal surface and demonstrate the relatively weak atomic modulation which is at the limit of the STM resolution. The two scans show very broad CDW maxima and the weak superimposed atomic modulation is quite variable. The majority of the z deflection occurs at the deep minima in the CDW superlattice as shown in the profiles of Fig. 15. These were

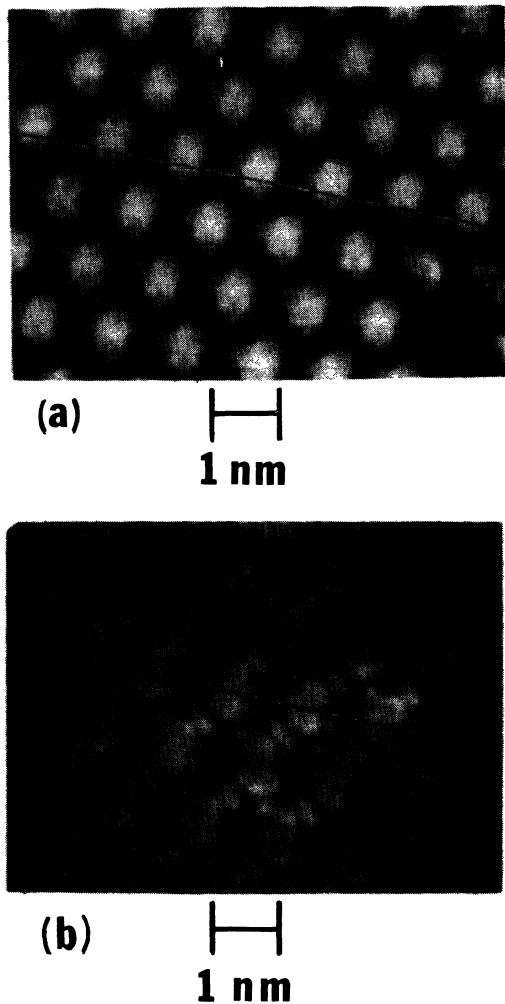


FIG. 14. Gray-scale images of STM scans on $1T\text{-TaSe}_2$ recorded at 4.2 K. The two scans were taken using the same tip-sample combination and demonstrate the dominant role of the CDW modulation relative to the weak superimposed atomic modulation. (a) The CDW maxima enhance seven-atom clusters ($I=2.2$ nA, $V=25$ mV). (b) The atomic modulation is extremely weak while CDW minima are strong and localized ($I=2.2$ nA, $V=25$ mV).

recorded along the traces shown in Fig. 14 and show a total z deflection of ~ 2.0 Å with the atoms contributing less than 0.25 Å to the deflection. The profiles shown in Fig. 15 demonstrate the nonsinusoidal shape of the CDW modulation as emphasized by the narrow width of the deep minima in the profile of Fig. 15(b). Comparison of the profiles in Figs. 15(a) and 15(b) also demonstrates the variable atomic resolution which results from the extreme dominance of the CDW modulation amplitude.

The large CDW deflections translate into relatively low barrier heights for $1T\text{-TaSe}_2$ and the characteristic tunneling curves reflect this fact. As shown in the I versus V and dI/dV versus V curves of Fig. 16 the presence of a ZBA can reduce the conductance below ~ 50 mV, but it remains relatively flat out to 150 mV. Above 150 mV the conductance shows a sharp rise and continues rising up

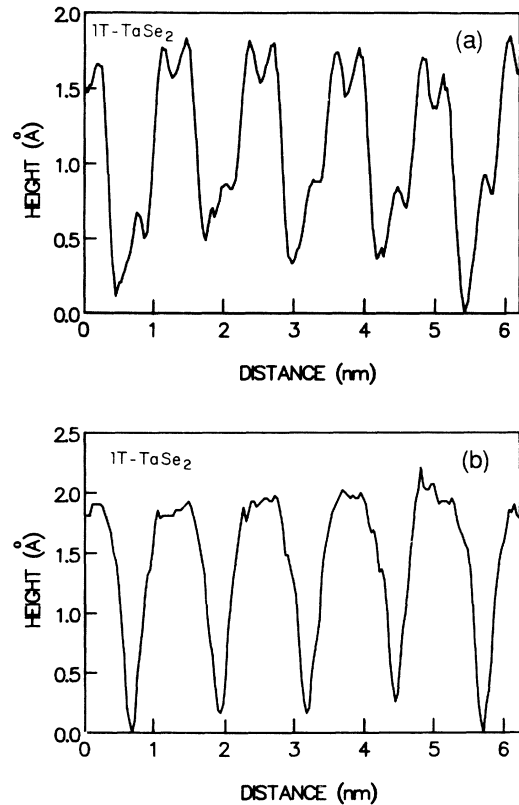


FIG. 15. (a) Profile of STM scan on $1T\text{-TaSe}_2$ recorded along track shown in Fig. 14(a). The total z deflection is ~ 2.0 Å with an atomic modulation ≤ 0.5 Å. (b) Profile of STM scan on $1T\text{-TaSe}_2$ recorded along track shown in Fig. 14(b). In this case the atomic modulation is barely visible and the nonsinusoidal shape of the CDW maxima indicates a nearly uniform z deflection over the central seven-atom cluster. A very narrow deep CDW minimum is also present.

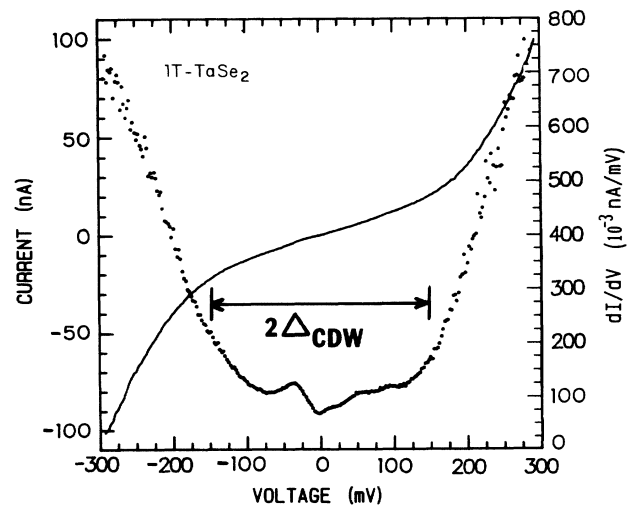


FIG. 16. Typical I vs V and dI/dV vs V curves measured for $1T\text{-TaSe}_2$ at 4.2 K. A sharp rise in conductance is observed at $\sim \pm 150$ mV which is identified with the CDW gap edge. A structure associated with a ZBA suppresses the conductance in the range ± 50 mV.

to the maximum applied bias. A rapid change in slope at 150 mV above the CDW gap edge is observed in all $1T$ -TaSe₂ crystals. This rapid conductance rise is characteristic of the low effective barrier height observed in $1T$ -TaSe₂ and demonstrated in Fig. 17.

Large z deflections and low effective barrier heights are generally observed for both $1T$ -TaSe₂ and $1T$ -TaS₂ and the characteristic curves in some cases can exhibit sizable ZBA's. However, selected crystal-tip combinations can show substantially lower z deflections and higher effective barriers. The I versus V and dI/dV versus V curves recorded from a higher barrier $1T$ -TaSe₂ junction are shown in Fig. 18. The effective barrier versus distance is shown in Fig. 19 and obtains a value of ~ 1.2 V at the set point of 75 mV and 2.2 nA. The conductance below ~ 150 mV is nearly constant with a value of ~ 0.030 nA/mV. Little or no ZBA is present in the higher barrier junction. A very rapid increase in conductance occurs at the CDW gap edge at ~ 150 mV. Previous tunneling measurements by Noutomi *et al.*¹⁰ carried out using $1T$ -TaSe₂-Al₂O₃-Al tunnel junctions at 4.2 K estimated Δ_{CDW} to be in the range 200–250 meV, substantially larger than is consistent with the present measurement.

In comparing the data from a range of crystal-tip combinations, we conclude that the CDW gap edge is at ~ 150 mV. The ZBA's correlate with enhanced z deflections and low barriers and also depress the conductance at low bias while an increased conductance is observed at intermediate bias voltages. The effect of a strong ZBA will be further demonstrated for $1T$ -TaS₂ as discussed below.

2. $1T$ -TaS₂

The characteristic tunnel curves of $1T$ -TaS₂ at 4.2 K are very similar to those observed for $1T$ -TaSe₂. However, the STM scans at 4.2 K do not give good atomic resolution and exhibit substantial instability when the tip is scanning. When the tip is held at a fixed position and dis-

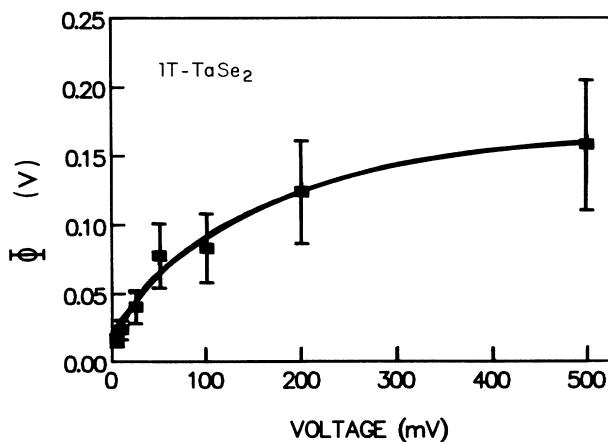


FIG. 17. A typical curve of effective barrier height vs bias voltage measured for $1T$ -TaSe₂ at 4.2 K. The effective barrier height remains below ~ 0.20 V over the entire range and decreases rapidly below ~ 100 -mV bias.

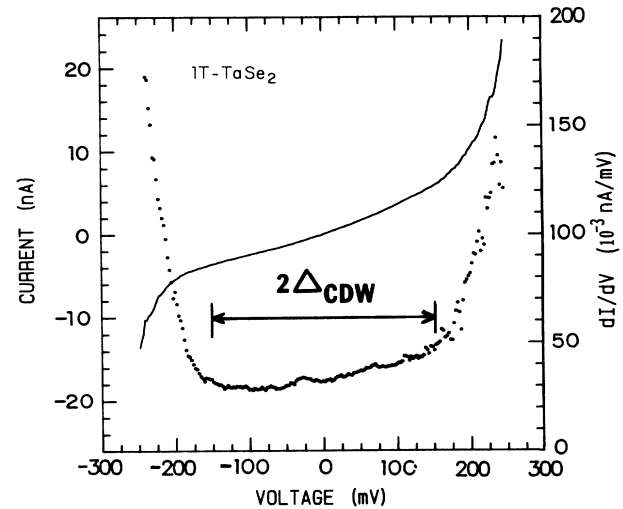


FIG. 18. I vs V and dI/dV vs V curves measured for $1T$ -TaSe₂ at 4.2 K using a tip-sample combination that did not exhibit a ZBA. A sharp slope change is again observed at $\sim \pm 150$ mV and the conductance below ± 150 mV is not suppressed by the ZBA as in the data of Fig. 16.

tance, the I versus V and dI/dV versus V curves are smooth and reproducible. This instability in the scanning mode may be associated with the onset of a metal-insulator transition known to occur in $1T$ -TaS₂ near 4.2 K. Local variations in the onset of this transition may affect the local density of states. In contrast, STM scans on $1T$ -TaS₂ at 77 K show excellent atomic resolution and no sign of instability. At 77 K comparison of the scans on $1T$ -TaSe₂ and $1T$ -TaS₂ show similar total z deflections of ~ 2 – 5 Å, but $1T$ -TaS₂ shows a consistently larger atomic modulation amplitude. In this paper we discuss

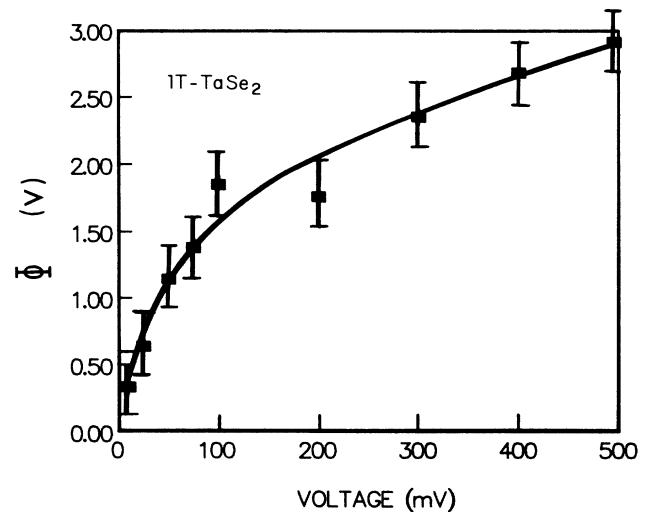


FIG. 19. Effective barrier height as a function of bias voltage measured for $1T$ -TaSe₂ using the tip-sample combination with no ZBA as shown in Fig. 18. At low bias the barrier height is a rapid function of bias, but rises quickly to a much higher value (> 2.0 V) than observed in junctions with ZBA's.

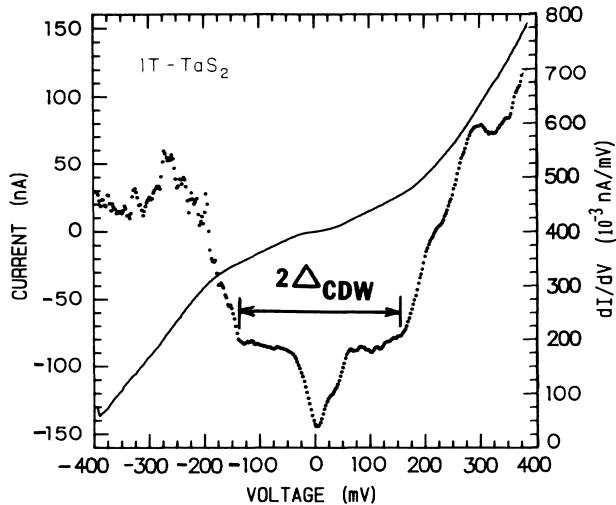


FIG. 20. I vs V and dI/dV vs V curves for $1T\text{-TaS}_2$ measured at 4.2 K. A sharp increase in conductance at $\sim \pm 150$ mV is again associated with the CDW gap edge. A ZBA extending to $\sim \pm 50$ mV is also observed, but does not interfere with the gap measurement.

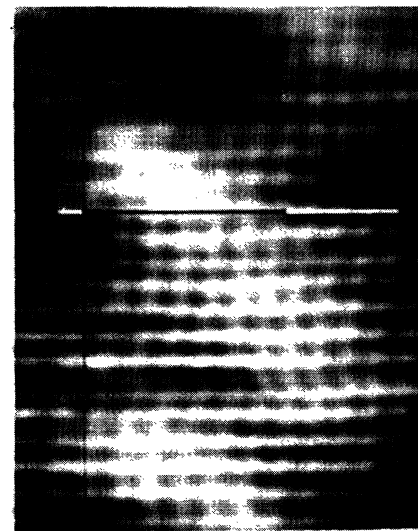
only the gap measurement using characteristic curves measured at 4.2 K.

Figure 20 shows I versus V and dI/dV versus V curves measured at 4.2 K for $1T\text{-TaS}_2$. The set point was again 75 mV and 2.2 nA and the effective barrier height was measured to be ~ 0.5 V. The curves show the presence of a strong ZBA extending to ~ 50 mV. However, this does not interfere with the observation of a sharp change in slope in the conductance curve at ± 150 mV corresponding to the CDW gap edge in $1T\text{-TaS}_2$.

C. Superconducting energy gap in $\text{Bi}_2\text{Sr}_2\text{CaCu}_2\text{O}_8$

The measurement of energy gaps in the high-temperature superconductors using STM has proven to be difficult. Atomic resolution at 4.2 K is obtained only on a relatively small percentage of samples and the characteristic tunneling curves show substantial variations in gap structure. Reproducible results have been obtained on $\text{Bi}_2\text{Sr}_2\text{CaCu}_2\text{O}_8$ single crystals which have been cleaved in air just before mounting in the STM followed by direct immersion in liquid helium.

The best gray-scale scans at 4.2 K show a well-resolved atomic structure as shown in the scan in Fig. 21(a). The surface is assumed to be BiO_x , consistent with the expected cleavage plane in Bi-Sr-Ca-Cu-O single crystals.¹¹ The measured atomic spacing in Fig. 21(a) is 4.0 ± 0.3 Å in approximate agreement with the x-ray structure determination of 3.8 Å for either the O-O or Bi-Bi spacing in the a - b plane. The z deflection shows the presence of different relative heights as indicated by the bright areas near the center of Fig. 21(a). A profile including this region is shown in Fig. 21(b). The bright area represents a broad maximum in apparent surface height while the individual atomic modulation amplitude of ~ 0.3 Å remains constant along the profile. This response can result from a variation in local electronic structure in the layers below



(a) 1 nm

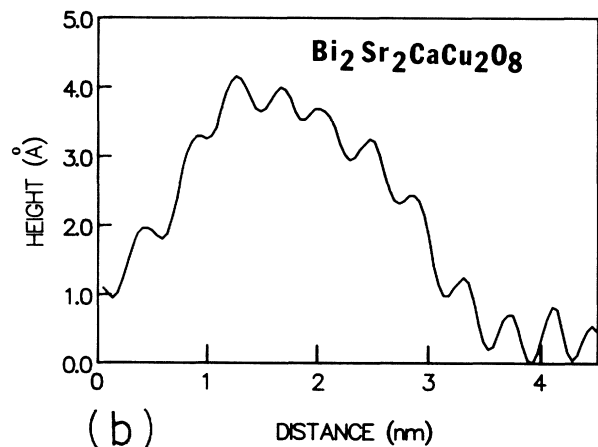


FIG. 21. (a) Gray-scale image of STM scan at 4.2 K on the BiO_x layer of a $\text{Bi}_2\text{Sr}_2\text{CaCu}_2\text{O}_8$ single crystal. The measured atomic spacing is 3.9 ± 0.3 Å. The bright areas correspond to areas of enhanced z deflection with no increase in the atomic modulation amplitude. (b) Profile along the track indicated in (a). The atomic modulation is ~ 0.5 Å and is continuous through the region of enhanced z deflection.

the surface as opposed to specific atomic defects or adsorbates associated with the surface layer. Further analysis and improvement in atomic resolution will be required before any conclusive information on the atomic structure can be derived. Chains of atoms with a long-range modulation of nine to ten unit cells can be seen in Fig. 21(a) and will be discussed further in Sec. IV.

The I versus V and dI/dV versus V curves generally show the presence of a strong gap structure, but the width and shape of this structure is strongly influenced by variations in the density of states below the gap edge

as well as variations in the position of the gap edge. These variations can occur during a series of runs at the same point on the surface or when recording characteristic curves from different positions on the surface.

The most stable characteristic curves show an effectively zero slope in the I versus V curve near zero bias and a very low density of states within the gap as shown in Figs. 22 and 23. The I versus V curve shows a very sharp onset of current at $\sim \pm 30$ mV, although this can show some asymmetry relative to zero bias. The corresponding conductance curve as shown in Fig. 23 indicates a very low density of states within the gap. The overall shape follows a BCS type of dependence but the position of the peak above the gap edge can be influenced by strong structure possibly associated with phonons just above the gap edge. The solid line drawn in Fig. 23 is a fit to a BCS-like density-of-states function as given in Eq. (5):

$$dI/dV = \text{Re} \frac{eV - i\Gamma}{[(eV - i\Gamma)^2 - \Delta^2]^{1/2}}, \quad (5)$$

where Γ is a broadening parameter representing mechanisms such as scattering associated with defects or inhomogeneities that introduce tunneling states below the gap. The solid line fit requires a value of 5.0 meV for Γ and a value of 37.9 meV for Δ . In comparing the two characteristic curves in Figs. 22 and 23 we estimate the gap to be in the range 30–35 meV. The conductance peak is clearly influenced by strong structure just above the gap edge which will increase the voltage at which the conductance peak occurs. Using values of $\Delta = 35$ meV and $T_c = 95$ K gives a value of $2\Delta/k_B T_c = 8.5$.

An I versus V curve taken on a different Bi-Sr-Ca-Cu-O single crystal over a range of current densities which are approximately five times lower than used for the data of Figs. 22 and 23 is shown in Fig. 24. The overall shape

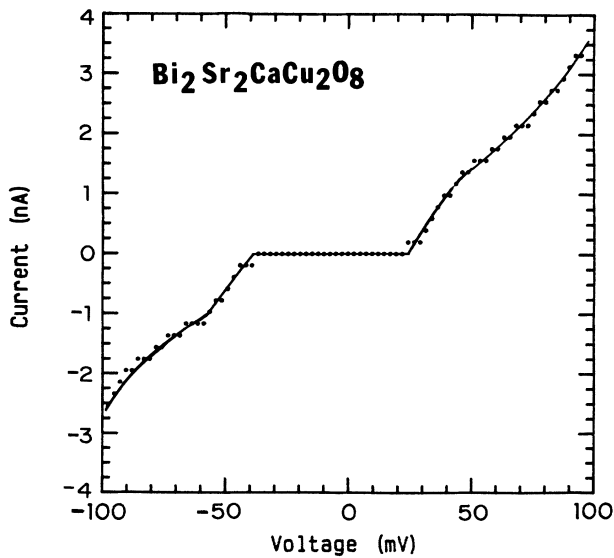


FIG. 22. I vs V curve measured on $\text{Bi}_2\text{Sr}_2\text{CaCu}_2\text{O}_8$ at 4.2 K. A zero slope is observed in the range of $\sim \pm 30$ mV with a well-defined onset of current above ± 30 mV. Some asymmetry is often observed, but is relatively small in the best junctions.

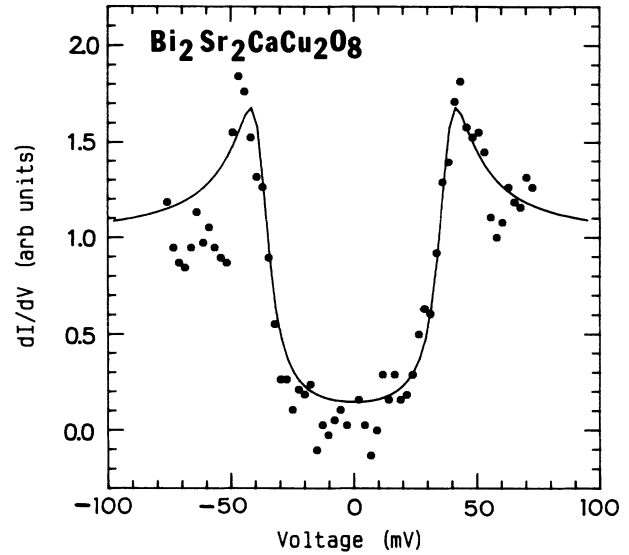


FIG. 23. Measured dI/dV vs V curve for $\text{Bi}_2\text{Sr}_2\text{CaCu}_2\text{O}_8$ crystal used for the data of Fig. 22 (solid points). Solid line is a fit to a BCS-type density of states given by $dI/dV = \text{Re}(eV - i\Gamma)/[(eV - i\Gamma)^2 - \Delta^2]^{1/2}$ where Δ is the energy gap and Γ is a broadening parameter. Values used to calculate the solid line are $\Delta = 38$ meV and $\Gamma = 5$ meV. A relatively low density of states is observed within the gap.

is the same as observed at higher currents, but the onset of current occurs at a slightly lower bias and the intermediate maximum above the gap edge is quite strong on the positive bias side. This structure occurs at 40–50 mV and can clearly influence the location of the peak in the corresponding conductance curve. This asymmetry of

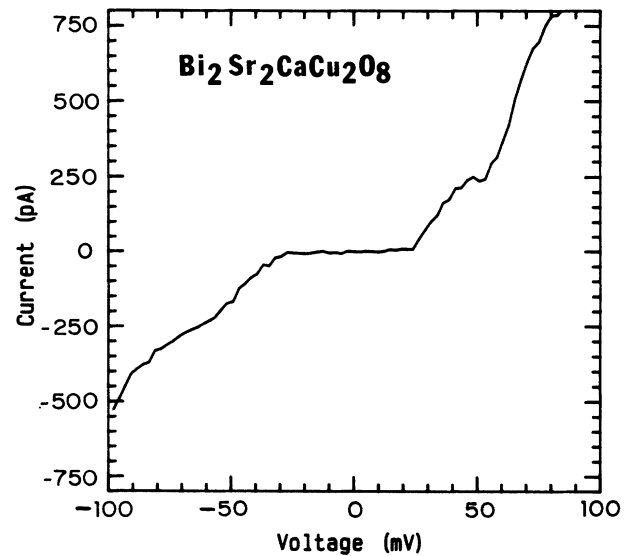


FIG. 24. I vs V curve measured on a second $\text{Bi}_2\text{Sr}_2\text{CaCu}_2\text{O}_8$ crystal with the set point chosen to give a current range five times lower than for the data of Fig. 22. The gap edge is again observed at $\sim \pm 30$ mV. An intermediate peak is observed at 40–50 mV and shows substantial asymmetry for positive and negative bias voltages.

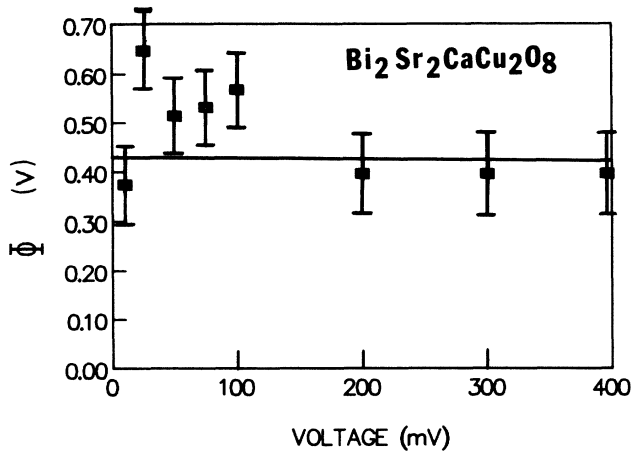


FIG. 25. Effective barrier height vs bias voltage measured for $\text{Bi}_2\text{Sr}_2\text{CaCu}_2\text{O}_8$ at 4.2 K. The barrier is ~ 0.45 V and remains nearly constant over the range 0–400 mV in contrast to the rapid rise observed in the layer-structure dichalcogenides.

the structure between positive and negative bias is commonly observed and a similar structure has been seen in Y-Ba-Cu-O junctions.⁵ The crystal used for these data exhibited zero resistance at 90 K and may have some phase mixture although it is dominantly composed of the 2:2:1:2 phase of Bi-Sr-Ca-Cu-O.

The effective barrier heights calculated from Eq. (4) show consistently low values below 1 V. However, in contrast to the results on the layer-structure dichalcogenides the effective barrier height is not a function of barrier thickness. A typical result is shown in Fig. 25 where low-voltage set points give the same effective barrier height as high-voltage set points. This suggests that the properties of the surface layer may be quite different than observed for the dichalcogenides where the surface layers are relatively good metals. This point will be discussed further in Sec. IV.

IV. DISCUSSION

The STM can be used to successfully measure energy gaps due to CDW formation and superconductivity in layered crystals. Structure in both the I versus V and dI/dV versus V curves can be used to determine the magnitude of these gaps. However, the junctions formed by the tunneling tip and the cleaved crystal surface exhibit a high sensitivity to small variations in either the microscopic tip geometry or possible impurities or defects within the junction interface or barrier. These produce substantial variations in the characteristic curves of I and dI/dV versus V , but do not directly affect the quality of the atomic resolution observed in the STM scans. However, the z deflections and the corresponding effective barrier heights can show significant changes correlated with variations observed in the characteristic curves. Accurate gap measurements should be made only on junctions exhibiting little or no ZBA structure. Low effective barrier heights and ZBA's can influence the tunneling response and the gap analysis must take this into account

although clear gap structure can still be present. The presence of low effective barrier heights and ZBA's in $2H\text{-TaSe}_2$ and $2H\text{-TaS}_2$ junctions can also substantially enhance the CDW amplitude. Table I lists the measured values of the CDW and superconducting gaps along with the value of T_c .

Systematic comparison of the results from the $2H$ -phase layer dichalcogenides gives CDW gap values of $\Delta_{\text{CDW}} \approx 80, 50,$ and 34 meV for $\text{TaSe}_2, \text{TaS}_2,$ and $\text{NbSe}_2,$ respectively. The calculated values of $2\Delta_{\text{CDW}}/k_B T_c$ for these values of Δ_{CDW} are 15.2, 15.4, and 23.9, all of them much larger than the weak-coupling BCS value of 3.53. The large values of $2\Delta_{\text{CDW}}/k_B T_c$ indicate that a strong electron-phonon coupling is involved in the CDW transition. In the case of $2H\text{-TaSe}_2$ and $2H\text{-TaS}_2$ the CDW induces a substantial modification of the Fermi surface and the CDW transitions are much stronger than the superconducting transitions which occur with very low T_c 's of 0.2 and 0.8 K, respectively. Values of $2\Delta_{\text{CDW}}/k_B T_c$ of ~ 15 for the CDW transitions indicate a very strong coupling, but are consistent for these two materials which exhibit similar experimental properties.

In the case of $2H\text{-TaSe}_2$ Barker *et al.*¹² have carried out infrared reflectivity studies and have identified a very weak gap structure with a threshold near 0.25 eV. This is a very large gap predicted on the basis of a very weak optical adsorption feature which would indicate removal of only about 1% of the FS. There might also be a range of gaps depending on the specific regions of the FS which are strongly coupled. The gap value of 0.08 eV measured in the present STM experiment is three times smaller, but still quite large relative to weak-coupling or long-coherence-length theories.

On the basis of the large gap measured by Barker *et al.*,¹² McMillan¹³ concluded that a short-coherence-length model was required in order to predict such a large gap. The estimated value of the coherence length was $\pi\xi_0 \approx 10$ Å, a value as short as is physically reasonable. The present gap value would not require such a short coherence length, but would still suggest the need for a short-coherence-length model. The gaps measured for $2H\text{-TaS}_2$ and $2H\text{-NbSe}_2$ are also larger than would be predicted by a long-coherence-length model, but quantitative comparisons are not available.

For $2H\text{-NbSe}_2$ the value of $2\Delta_{\text{CDW}}/k_B T_c = 23.9$ for the CDW transition seems unusually large since one might conclude that the Fermi-surface modifications and the effects on the physical properties induced by the CDW are weaker than for the Ta compounds. The CDW onset is substantially lower at 33 K and the superconducting

TABLE I. List of compounds and measured parameters.

Compound	T_c (K)	Δ (meV)	$2\Delta/k_B T_c$
$2H\text{-TaSe}_2$	122.3	80	15.2
$2H\text{-TaS}_2$	75.3	50	15.4
$2H\text{-NbSe}_2$	33	34	23.9
$1T\text{-TaSe}_2$	600	150	5.8
$1T\text{-TaS}_2$	600	150	5.8
$\text{Bi}_2\text{Sr}_2\text{CaCu}_2\text{O}_8$	95	30–35	7.3–8.5

transition is substantially higher at 7.2 K. The corresponding superconducting energy gap has been measured^{9,14,15} as $\Delta = 1.12$ meV, giving a value of $2\Delta/k_B T_c = 3.6$ for the superconducting transition, a value in agreement with the BCS weak-coupling limit. The coexistence of the CDW and superconducting phases at low temperature makes NbSe₂ a very special case. Raman scattering^{16,17} experiments at low temperature have shown that the Raman active CDW phonon modes are coupled to the superconducting gap excitations. Whether this has any relation to the large value of the CDW gap is unknown. NbSe₂ remains as an unusual case and supports the trend toward a short-coherence-length model for the 2H-phase materials.

The 1T-phase compounds 1T-TaSe₂ and 1T-TaS₂ both have onset temperatures estimated to be ~ 600 K. The pure 1T phases undergo polytypic transitions at ~ 550 K which interrupt an accurate determination of the onset temperature for the incommensurate CDW phase. On the basis of measurements¹⁸ on dilute Ti-doped samples in which the 1T phase is stabilized the onset temperature is estimated to be ~ 600 K. Using this value of T_c gives a value of $2\Delta_{\text{CDW}}/k_B T_c$ for both 1T-TaSe₂ and 1T-TaS₂ of 5.8, much smaller than observed for the 2H phases, but indicative of fairly strong coupling. At 4.2 K the gap edge is observed at ± 150 mV for both 1T-TaSe₂ and 1T-TaS₂.

Barker *et al.*¹² have also measured the infrared adsorption in 1T-TaS₂ as a function of temperature. They found a weak structure at 380 K suggesting a gap near 0.1 eV and also observed decreases in the transition strength at lower temperatures suggesting a range of gap energies. The present STM measurement of 0.15 eV is consistent with the range predicted by the optical data, but no specific values can be derived from the optical data. The values of $2\Delta/k_B T_c$ of ~ 5 found for the 1T-phase materials suggest that the short-coherence-length theories may not be required in this case.

The tunneling results obtained on Bi-Sr-Ca-Cu-O single crystals with the STM are sufficiently variable that deducing quantitative values of the gap by averaging is not significant. The largest problem seems to be a large variation in the apparent tunneling density of states below the gap edge and the presence of a variable nonzero conductance at zero bias. The data shown in Figs. 22–24 were selected as examples where these factors play a minimal role in that the I versus V curves show zero slope at zero bias and the conductance approaches zero at zero bias. In addition the broadening of the gap edges is sufficiently small that the lifetime broadening function used for low-temperature superconductors as given by Eq. (5) does not require an abnormally large value of Γ relative to Δ . A reasonably stable and nearly symmetric behavior was also observed.

The superconducting gap range of 30–35 meV derived from the data presented in Figs. 22–24 gives an average value of $2\Delta/k_B T_c \approx 8$. This value is slightly higher than reported by other tunneling experiments on Bi-Sr-Ca-Cu-O crystals and films which report values in the range 6–7, although all of these measurements give values of $2\Delta/k_B T_c$ a factor of 2 larger than the weak-coupling

BCS value. High-resolution angle-resolved photoelectron spectroscopy experiments^{19–22} on Bi-Sr-Ca-Cu-O single crystals report values of $\Delta = 30$ meV, consistent with the present tunneling measurement. High-resolution photoemission results¹⁸ on YBa₂Cu₃O₇ also are best fit by a gap giving $2\Delta/k_B T_c$ on the order of 8.

In contrast to the best tunneling data, other tip-sample combinations give I versus V curves with a nonzero slope at zero bias accompanied by conductance curves that show extreme broadening below the gap edges and a substantially zero-bias conductance. Standard analysis of the true gap values is then difficult even though structure and slope changes exist which seem to be identified with a fairly large gap.

For some tip-sample combinations the opposite effect is observed and the curves are characterized by very large gaps and a zero conductance over a large range of bias. Extremely sharp jumps are also observed at the apparent gap edge. Many of these gap structures are due to possible charging effects, to the presence of large ZBA's similar to those observed in some layer compound junctions, or to the possible presence of insulating or semiconducting particles in the junction. They often show large bias asymmetries or large changes from one voltage sweep to the next. Some of these large-gap structures may be due to tip-substrate combinations that measure 2Δ due to the formation of a S - I - S junction within the tip-surface geometry. These will generally be sharper than the S - I - N junctions which measure Δ , but it is difficult to separate these specific legitimate cases from the larger number of noninteger anomalous cases. A reasonably good example of a STM measurement on Bi-Sr-Ca-Cu-O that is probably a measurement of 2Δ was given by Kirk *et al.*²³ They originally interpreted it as Δ , but considering it as a measurement of 2Δ gives $\Delta = 27$ meV, in reasonably good agreement with the selected data shown here and with other STM measurements that give a large gap in Bi-Sr-Ca-Cu-O single crystals.

The reasons for the large variations in the characteristic curves observed for a series of tip-sample combinations prepared using the same procedure can involve a number of factors. The high- T_c superconductors have extremely short coherence lengths and any variation in gap size can occur on a length scale comparable to the decay of the electronic wave function away from the surface. The tunneling electron might therefore sample a region with different gap values. This is equally true if lateral gap inhomogeneities exist since small changes in tip geometry or distance between tip and surface could change the effective area of the junction. A short coherence length in the range below 10 Å would enhance all such gap inhomogeneities.

Studies of the cleaved surface of Bi-Sr-Ca-Cu-O single crystals generally conclude that the top surface is the Bi-O plane. The states near the Fermi level are believed to be primarily oxygen p states so that the STM scans such as the one shown in Fig. 21(a) image only the oxygen atoms when the scan is run at relatively low voltages [100 meV for Fig. 21(a)]. The measured spacing of ~ 4 Å is consistent with imaging only one type of atom in the Bi-O plane. The scan in Fig. 21(a) also shows chains of

atoms similar to those observed by Shih *et al.*²⁴ with STM scans on Bi-Sr-Ca-Cu-O single crystals at room temperature. In addition these chains show a modulation along the chain axis which appears to be very similar to that observed by Shih *et al.*²⁴ They observed a modulation period of nine to ten unit cells and analyzed it in terms of compressive and expansive atomic displacements along the *a* axis. The STM scan is 4.2 K in Fig. 21(a) is consistent with this result, but the image quality is not sufficient for quantitative measurement of the modulation. In addition, we do not observe missing atoms in any of the profiles which have been run. In this respect we agree with Shih *et al.*²⁴ and have not observed structure such as that observed by Kirk *et al.*²³ which they interpreted as missing atoms. Our atomic modulation amplitude is ~ 0.3 Å in approximate agreement with that observed at room temperature by Shih *et al.*²⁴

The spectroscopic STM studies at room temperature by Shih *et al.*²⁴ concluded that there was a zero density of states at the Fermi level and that the Bi-O layer might not be metallic. We have not carried out any extensive spectroscopic measurements at 4.2 K and at this stage cannot draw any definite conclusions. The STM scans on Bi-Sr-Ca-Cu-O crystals clearly require higher voltages than needed for the layer dichalcogenides consistent with a much lower density of states at the Fermi level.

The effect of this low density of states on the STM scans and the characteristic tunneling curves has not been fully explored. If the metallic states exist only in layers below the surface, then there is danger that the tip contacts the surface, or that the current signal from the metallic states is too small to provide good gap structure. The effective barrier height remains relatively constant as a function of thickness (see Fig. 25). This might suggest that a part of the surface layer contributes to the insulating barrier preventing the effective barrier height from decreasing rapidly as the tip approaches the surface as occurs in the layer-structure dichalcogenides. Either of these effects would limit the quality and reproducibility of the data obtained from the STM.

The gap measurement of $\Delta = 30\text{--}35$ meV in the present experiment is of course made with the tip perpendicular to the *a-b* plane. If there is gap anisotropy present then the larger gap would be expected to occur parallel to the *a-b* plane. However, the extreme geometry of the tip-substrate junction and the presence of a very low tunnel barrier can easily give a tunnel current that comes from a combination of carriers tunneling parallel and perpendicular to the direction of the large gap. The observed gap structure could therefore be dominated by the larger gap, although sufficiently good data would be expected to detect the smaller gaps as well.

V. CONCLUSIONS

A scanning tunneling microscope operating in a bath of liquid helium has been successfully used to measure energy gaps in charge-density-wave materials and in high-temperature superconductors. Structures in the *I* versus *V* and *dI/dV* versus *V* characteristic curves have been identified with the energy gap. STM scans with atomic

resolution have also been obtained on the same crystal surfaces. All of the surfaces studied were prepared by cleaving the quasi-two-dimensional crystals in air just before introducing the STM into helium gas and then cooling to 4.2 K. In the case of the layer-structure dichalcogenides good atomic resolution can be obtained relatively easily while the characteristic spectroscopic curves show well-defined variations even though good atomic resolution is maintained.

We have shown that the CDW gap structure in *2H*- and *1T*-phase layer dichalcogenides can be identified in the STM conductance curves. This structure is systematically reproducible along with other junction characteristics such as *z* deflection, effective barrier height, and the magnitude of the conductance. Variations from the standard behavior are observed and these are correlated with the presence and strength of the ZBA's observed in the tunnel conductance as a function of bias voltage. By running a series of *2H*-phase crystals we have shown that the ZBA's can be reduced for selected tip-sample combinations and a reasonably accurate determination of the CDW gap can be made. Values of Δ_{CDW} for *2H*-TaSe₂, and *2H*-NbSe₂ are 80, 50, and 34 meV, respectively. For all three *2H*-phase crystals studied the values of $2\Delta_{\text{CDW}}/k_B T_c$ are in the range 15–24 and are very large relative to the weak-coupling BCS value of 3.53. *2H*-NbSe₂ is particularly unusual in that it exhibits a low CDW onset temperature of ~ 33 K and a relatively high superconducting transition temperature of ~ 7 K, while showing the highest value of $2\Delta_{\text{CDW}}/k_B T_c = 23.9$. All three *2H*-phase materials indicate a trend toward a short-coherence-length model.¹³

The conductance curves measured for the *1T*-phase compounds show a well-defined CDW gap structure at ~ 150 mV giving values of $2\Delta_{\text{CDW}}/k_B T_c$ on the order of 5 which suggests relatively strong coupling, but not unusually large as in the case of the *2H* phases. We have also shown that junctions with little or no ZBA structure can be produced with the *1T*-phase materials, but that the presence of ZBA's does not interfere or change the CDW gap structure. When present we have shown that the ZBA strength correlates with a reduced conductance and an enhanced *z* deflection in the STM scan.

In the *2H*-phase compounds a weaker CDW gap structure is observed and junctions with little or no ZBA structure can also be produced. However, when ZBA strength is present care must be taken in measuring the CDW gap structure since the ZBA can overlap the CDW gap structure although no shift in the CDW gap edge is induced.

The layer-structure dichalcogenides with the strongest CDW's show the largest total *z* deflections and consequently the lowest effective barrier heights. When ZBA's are present a further enhancement of the *z* deflection is observed leading to a corresponding lowering of the effective barrier height. In addition, the effective barrier height measured for each of the layer-structure dichalcogenides shows a strong decrease as the tip-sample distance is reduced. For the characteristic curves analyzed in this paper an intermediate distance has been chosen by using an initial set point of 75 mV and 2.2 nA to set the

tip-sample distance.

STM scans from the tip-sample combinations and procedures described in this paper show consistent and reproducible z deflections, barrier heights, and conductance curves. The characteristic z deflections are in the range 0.5–1 Å for the $2H$ -phase layer dichalcogenides and in the range 2–3 Å for the $1T$ -phase layer dichalcogenides with the latter showing a dominant CDW structure compared to the $2H$ -phase compounds where the CDW structure is comparable to or less than the atomic structure. The corresponding barrier heights are therefore systematically less in the $1T$ compounds than in the $2H$ compounds. In all cases the barrier heights are very low at small tip-sample distances and rise rapidly at larger distances with an indication of saturation at large distance. Tip-sample combinations with the above characteristics are reproducible and give reasonable gap structure for all of the layer-structure dichalcogenides studied. When ZBA's are present the conductance is decreased, the z deflection is increased, and the barrier height is decreased at a given tip-sample distance. The functional dependence of the barrier height versus tip-sample distance is, however, similar to that observed in the junctions without ZBA's.

The results show that the characteristic curves, the effective barrier heights, and the magnitude of the conductance at a given tip-sample spacing are a much more sensitive measure of the precise junction condition than is the observation of atomic structure. Detailed analysis and spectroscopy therefore require tests on a large number of junctions before all characteristic structures can be identified. This is particularly true for Bi-Sr-Ca-Cu-O single crystals where the characteristic curves can show an extremely wide variation. Although we have been successful in identifying a strong gap structure in Bi-Sr-Ca-Cu-O single crystals we have not developed a good technique for forming junctions that show a consistently reproducible gap structure. The best junctions indicate a superconducting gap of 30–35 meV with values of $2\Delta/k_B T_c$ of ≈ 8 .

Measurements of STM junctions in an UHV environment with ultraclean surfaces would be useful for comparison to the present data and should eventually be carried out. However, the layer-structure dichalcogenides cannot be baked at very high temperature without loss of S or Se and preparation of sufficiently clean vacuum conditions for useful experiments will be difficult. After a large number of experiments using the cleaved substrates in helium gas and liquid helium the reproducibility and consistently excellent resolution of atomic and CDW structure indicate that surface contamination is not a ma-

ior variable. The variations in STM response that occur for our tip-sample combinations appear to be a function of specific tip geometries or of defects or impurities at or near the tip. Changing the tip or touching the surface with the tip can change the characteristic curves subsequently measured on the same substrate. This is particularly true with respect to the strength of any observed ZBA. The present Pt-Ir tips are prepared by mechanical machining and no control of detailed atomic structure has so far been attempted. Experiments with different tip preparation techniques are underway. The presence of particles, impurities, or defects at the position of the tip or on the tip can introduce large ZBA's or Coulomb blockade effects.²⁵ This can interfere with accurate spectroscopy measurements, but can be controlled by systematic studies on a large number of tip-sample combinations.

With the present preparation techniques we feel that the STM junctions have been systematically characterized and exhibit sufficient reproducibility to allow accurate measurement of the CDW gap structure. The presence of ZBA's and their possible effects on the gap measurements have been analyzed. We also have shown a correlation between the ZBA strength and the amplitude of the observed z deflection and the magnitude of the effective barrier height. The analysis of these correlations provides a further useful way to systematically characterize and define a specific STM tip-substrate combination and its suitability for measuring energy-gap structure.

The results show that the STM can be used to obtain useful and reliable gap measurements. It has the advantage of measuring a very localized junction area and of not requiring an artificial barrier to be formed. At the same time the extreme junction geometry seems to be more sensitive to small variations in either the effective junction area, the substrate conditions, or contamination at the junction interface. This is reflected in variations of effective barrier height. More work needs to be done in order to understand the sources of these variations, but useful systematic information can be obtained from the present data.

ACKNOWLEDGMENTS

This research has been supported by the U.S. Department of Energy under Grant No. DE-FG05-84-ER45072. The authors have benefited from useful discussions with Vittorio Celli, Paul Hansma, Joe Demuth, and Andy Johnson. Barney Drake has contributed to the design and construction of the STM's.

¹R. V. Coleman, B. Giambattista, P. K. Hansma, A. Johnson, W. W. McNairy, and C. G. Slough, *Adv. Phys.* **37**, 559 (1988).

²R. E. Thompson, U. Walter, E. Ganz, J. Clarke, A. Zettl, P. Raunch, and F. J. DiSalvo, *Phys. Rev. B* **38**, 10 734 (1988).

³X. L. Wu and C. M. Lieber, *Science* **243**, 1703 (1989).

⁴B. Giambattista, A. Johnson, and R. V. Coleman, *Phys. Rev. B*

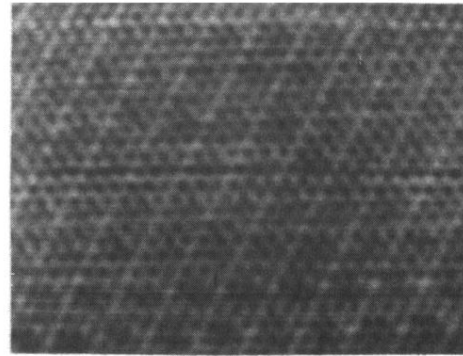
37, 2741 (1988).

⁵J. R. Kirtley, *Int. J. Mod. Phys. B* **4**, 201 (1990).

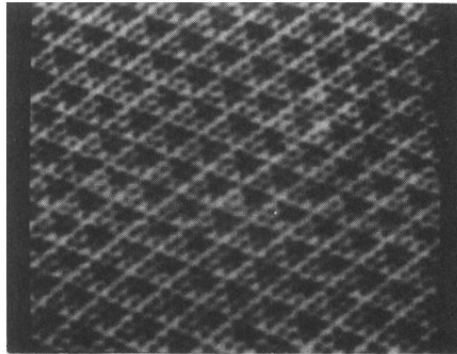
⁶J. A. Wilson, F. J. DiSalvo, and S. Majahan, *Adv. Phys.* **24**, 117 (1975).

⁷S. J. Hillenius and R. V. Coleman, *Phys. Rev. B* **18**, 3790 (1978).

- ⁸J. E. Graebner and M. Robbins, *Phys. Rev. Lett.* **36**, 422 (1976).
- ⁹H. F. Hess, R. B. Robinson, R. C. Dynes, J. M. Valles, Jr., and J. V. Waszczak, *Phys. Rev. Lett.* **62**, 214 (1989).
- ¹⁰S. Noutomi, T. Fatatsugi, M. Naito, and S. Tanaka, *Solid State Commun.* **50**, 181 (1984).
- ¹¹P. A. P. Lindberg, Z. X. Chen, B. O. Wells, D. Dessau, D. B. Mitzi, I. Lindau, W. E. Spicer, and A. Kapitulnik, *Phys. Rev. B* **39**, 2890 (1989).
- ¹²A. S. Barker, Jr., J. A. Ditzenberger, and F. J. DiSalvo, *Phys. Rev. B* **12**, 2049 (1975).
- ¹³W. L. McMillan, *Phys. Rev. B* **16**, 643 (1977).
- ¹⁴R. C. Morris and R. V. Coleman, *Phys. Lett.* **43A**, 11 (1973).
- ¹⁵B. P. Clayman and R. F. Frindt, *Solid State Commun.* **9**, 1881 (1971).
- ¹⁶R. Sooryakumar and M. V. Klein, *Phys. Rev. Lett.* **45**, 660 (1980).
- ¹⁷R. Sooryakumar and M. V. Klein, *Physica* **105B**, 422 (1981).
- ¹⁸F. J. DiSalvo, J. A. Wilson, B. G. Bagley, and J. V. Waszczak, *Phys. Rev. B* **12**, 2220 (1975).
- ¹⁹Y. Chang, Ming Tang, R. Zandoni, M. Onellion, R. Joynt, D. L. Huber, G. Margaritondo, P. A. Morris, W. A. Bonner, J. M. Tarascon, and N. G. Stoffel, *Phys. Rev. B* **39**, 4740 (1989); *Phys. Rev. Lett.* **63**, 102 (1989).
- ²⁰J. M. Imer, F. Patthey, B. Dardel, W.-D. Schneider, Y. Baer, Y. Petroff, and A. Zettl, *Phys. Rev. Lett.* **62**, 336 (1989).
- ²¹R. Manzke, T. Buslaps, R. Claesen, and J. Fink, *Europhys. Lett.* **9**, 477 (1989).
- ²²C. G. Olson, R. Liu, A. B. Yang, D. W. Lynch, A. J. Arko, R. S. List, B. W. Veal, Y. C. Chang, P. Z. Jiang, and A. P. Paulikas, *Science* **245**, 731 (1989).
- ²³M. D. Kirk, C. B. Eom, B. Oh, S. R. Spielman, M. R. Beasley, A. Kapitulnik, T. Geballe, and C. F. Quate, *Appl. Phys. Lett.* **52**, 2071 (1988).
- ²⁴C. K. Shih, R. M. Feenstra, J. R. Kirtley, and G. V. Chandrasekhar, *Phys. Rev. B* **40**, 2682 (1989).
- ²⁵D. V. Averin and K. K. Likharev, *J. Low Temp. Phys.* **62**, 345 (1986).

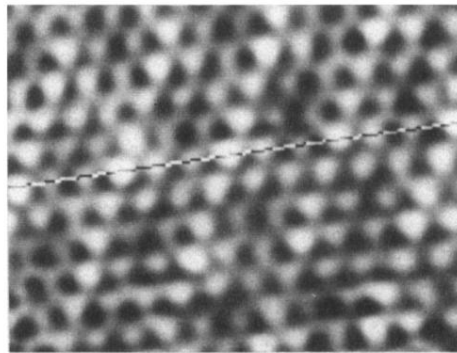


(a) 
1 nm

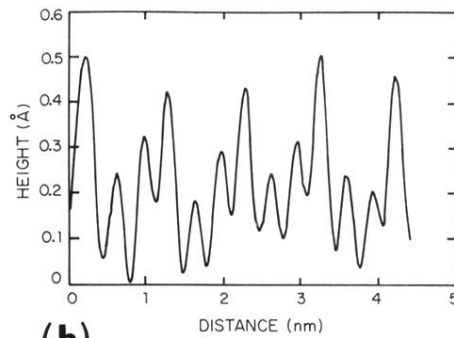


(b) 
1 nm

FIG. 1. Gray-scale images of STM scans on two different crystals of $2H\text{-TaSe}_2$ at 4.2 K. The two images show the CDW as an enhancement on every third row of atoms, but differ in total z deflection by a factor of 8 as indicated in the profiles shown in Fig. 2. (a) Scan taken at $I=2.2$ nA and $V=25$ mV. (b) Scan taken at $I=2.2$ nA and $V=75$ mV showing an enhanced CDW modulation and a larger total z deflection.

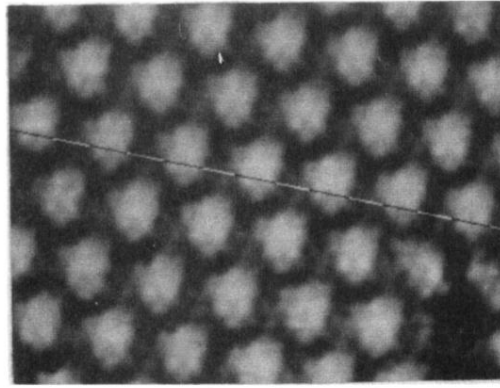


(a) 
1 nm

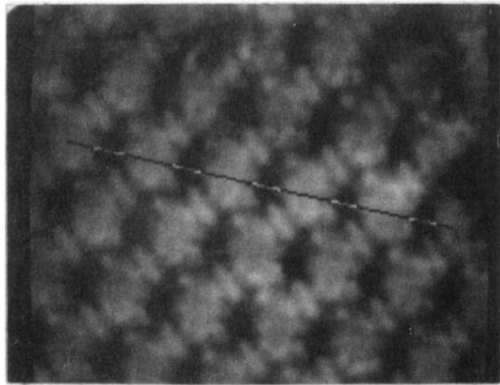


(b)

FIG. 10. (a) Gray-scale image of STM scan on $2H\text{-NbSe}_2$ at 4.2 K. ($I=2.0$ nA, $V=25$ mV). The total z deflection is low at ~ 0.5 Å with CDW and atomic modulations of approximately equal magnitudes as shown in the profile in (b) (from Ref. 10).

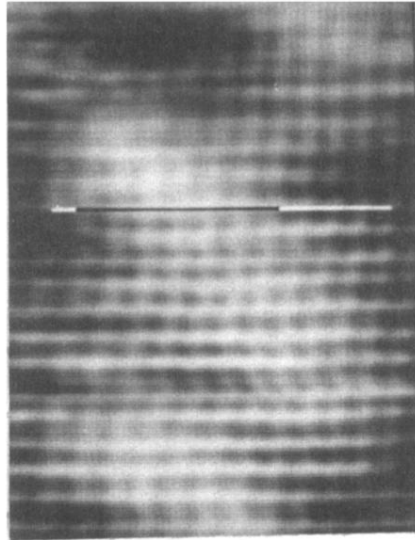


(a) 
1 nm



(b) 
1 nm

FIG. 14. Gray-scale images of STM scans on $1T\text{-TaSe}_2$ recorded at 4.2 K. The two scans were taken using the same tip-sample combination and demonstrate the dominant role of the CDW modulation relative to the weak superimposed atomic modulation. (a) The CDW maxima enhance seven-atom clusters ($I=2.2$ nA, $V=25$ mV). (b) The atomic modulation is extremely weak while CDW minima are strong and localized ($I=2.2$ nA, $V=25$ mV).



(a) 
1 nm

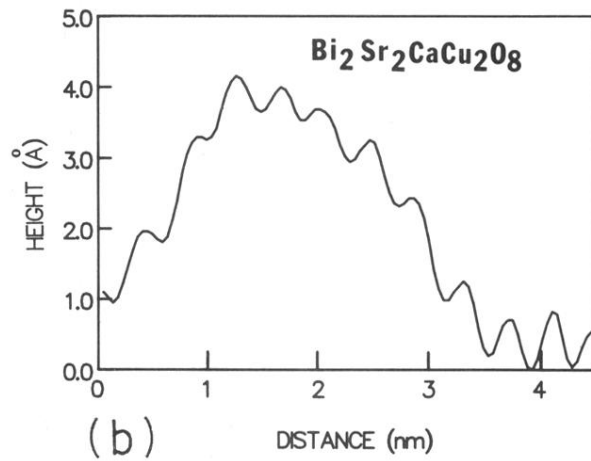


FIG. 21. (a) Gray-scale image of STM scan at 4.2 K on the BiO_x layer of a $\text{Bi}_2\text{Sr}_2\text{CaCu}_2\text{O}_8$ single crystal. The measured atomic spacing is $3.9 \pm 0.3 \text{ \AA}$. The bright areas correspond to areas of enhanced z deflection with no increase in the atomic modulation amplitude. (b) Profile along the track indicated in (a). The atomic modulation is $\sim 0.5 \text{ \AA}$ and is continuous through the region of enhanced z deflection.